Proceedings of Global Power and Propulsion Society
ISSN-Nr: 2504-4400
GPPS Chania20
7th – 9th September, 2020
www.gpps.global

GPPS-CH-2020-#108

Nonlinear mode interaction effects in the vibration of bladed-disks

Salvador Rodríguez
Universidad Politécnica de Madrid
salvador.rodriguez@upm.es
Madrid, Spain

Carlos Martel
Universidad Politécnica de Madrid
carlos.martel@upm.es
Madrid, Spain

ABSTRACT

Nonlinear mode interaction caused by friction at blade-root attachments is a common phenomenon in current bladed-disk configurations. However, it is still far from been completely understood, and the application of simple linear superposition can lead to an overestimation of the system vibrational response. In this work, nonlinear mode interaction is analyzed using a simplified mass-spring model with a microslip friction model. The parameters of the model are set using data from actual experimental results from a realistic bladed-disk, which are rarely available. Two different configurations are considered. The interaction of the synchronous response of the system due to harmonic excitation with a non-synchronous aerodynamically unstable mode, and the interaction of two synchronous harmonic excitations with similar frequencies and different engine orders.

INTRODUCTION

Aeroelastic vibration of turbomachinery has brought the attention of both the industry, because of the elevated costs derived from it (see for example (Cowles, 1996) for a study of the costs associated to HCF), and the academia, because of the reach dynamics obtained (see for example (Krack et al., 2017) for a review of the problem). However, despite all the effort made, the problem is still far from being completely understood, among other things, because of the expensive costs of both its experimental and computational study.

That is the reason why dedicated experiments on realistic configurations are rarely performed. On the contrary, simplified configurations are tested or, when realistic geometries are used, clearing the hardware for certification and service is the main goal. Some of these few experiments were performed as part of the European project "Flutter-Free Turbomachinery Blades" FUTURE (http://www.future-project.eu/, 2008-2012) for both flutter and forced response (see, (Corral et al., 2013) for a condensed description of the results of the FUTURE experiments).

The high computational cost of the problem is associated to its interdisciplinary nature. For its correct simulation, the whole set of solid equations for the structure and fluid equations for the surrounding gas need to be considered. Additionally, the dry friction of the contacting parts of the assembly (shroud, friction damper, blade-root attachment), although small in general, is the main source of energy dissipation and it has to be taken into account. This increases the cost considerably because of its nonlinear nature and the slow time scales that appear due to its relatively small value (see (Yang et al., 1998) and (Yang and Menq, 1998)).

Although some simplification can be considered (it is common to assume a semi-uncoupled approach with linearized aerodynamic forces (see for example (Corral and Gallardo, 2013)), and a multi-harmonic balance method to solve the problem in the frequency domain (see for example (Petrov and Ewins, 2004))), this is still an expensive problem in practice. Because of this, different reduced order models (ROMs) have been developed and used to get an insight into the system behavior and the main physical mechanism (see for example (Gross and Krack, 2019)).

Depending on their nature, there are two main types of problems in aeroelasticity of turbomachinery: the forces response problem, where an external force causes the vibration of the system (the pulsating aerodynamic forces produced by the wakes of the upstream stator of the engine are a typical source of excitation), and the flutter problem, where the vibration is the result of a stability problem without the action of any external force. In the case of forced response, the final nonlinear limit cycle oscillation that sets in the rotor shows the same frequency and engine order as the external forcing, see (Petrov and Ewins, 2003 and 2004) for an explanation of the calculation procedure using a high fidelity FEM, and see also (Martel and Martín, 2020) for an asymptotically simplified description of the nonlinear friction saturation of the vibration amplitude. Flutter, on the other hand, is a more complex phenomenon in which several unstable TW modes can be present simultaneously, and currently, there is not a definitive answer about the nature of the final vibration state

that appears for large times. It is not clear whether it is composed of several TWs or just one TW, the most unstable one (see Gross and Krack, 2019, for a recent description of the problem, and Martel et al., 2014, for an asymptotic analysis).

Most studies have been restricted to the analysis of one of these phenomena separately without considering their combination. But, due to the nonlinearity introduced by the friction forces, the simple linear superposition of the separated effects does not represent the combined response of the system. The conceptual analysis of combined flutter and forced response presented in (Corral and Gallardo, 2013) showed that the nonlinear interaction of the excited modes changes drastically the output of the system, inhibiting completely the flutter instability when the forcing frequency is close to the resonance. Because of this, one of the main objectives of the European project Advanced Research Into Aeromechanical Solutions ARIAS (https://www.arias-project.eu/, 2018-2022), where this work is framed, is to understand nonlinear vibration mode interaction. Two experiments of nonlinear mode interaction in a realistic LPT rotor will be carried out in this project: one will test the combined effect of flutter and forced response in a high speed wind tunnel, and another one will study the interaction of two different forcings in an in-vacuum spin pit. The purpose of the results of this paper is to support the design of these experiments using a conceptual rotor model to explore the system response with both configurations.

For this, a mass-spring model with 3 DOF per sector is used to study the nonlinear modal. This type of models has been successfully used in previous works because of their low computational requirements (Sinha, 2017). The model parameters (elastic, aerodynamic, and friction) are calibrated using actual experimental data from a low-pressure turbine from the FUTURE European project. Both mode interactions are studied: the interaction produced by the superposition of forced response and flutter, and the interaction of two forcings of modes of the same family with different engine orders. Another objective is to compare both types of mode interaction, to assess the possibility to study flutter and forced response interaction in an in-vacuum spin-rig by mean of two forced responses, one of which would have an engine order similar to the expected flutter.

The paper is organized as follows; in the next section, the lumped model and the selection of parameters are described. Afterward, the analysis of the forced response and flutter interaction is presented, followed by the study of the interaction of two forced responses acting on the same modal family. Finally, the main conclusions are summarized in the last section.

ROM DESCRIPTION AND PARAMETER SELECTION

In this section, the reduced order model used is described, as well as the parameters selected to match the experimental measurements obtained in the FUTURE project.

A sketch of the mass-spring model is presented in figure 1.

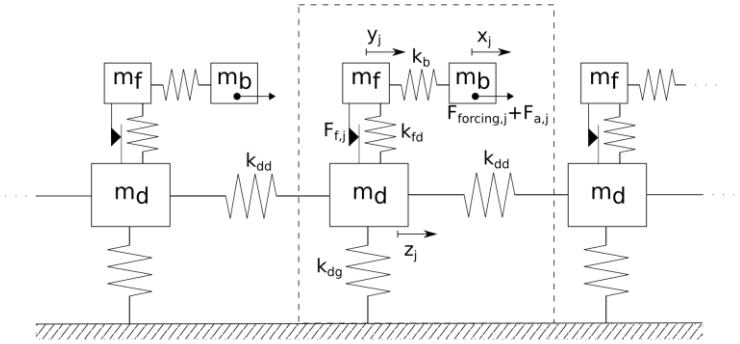

Figure 1 Sketch of the lumped model

The 3 DOFs per sector correspond to; the blade displacement, x_i, the friction dynamics at the fir-tree, y_i, and the disk sector displacement, z_i. The equations for a single sector, j, can be expressed as:

$$\begin{aligned} m_b \frac{d^2 x_j}{dt^2} + k_b(x_j - y_j) &= F_{a,j} + F_{forcing,j} \\ m_f \frac{d^2 y_j}{dt^2} + k_b(y_j - x_j) + k_{fd}(y_j - z_j) + F_{f,j}(y_j - z_j) &= 0 \\ m_d \frac{d^2 z_j}{dt^2} + k_{dd}(-z_{j+1} + 2z_j - z_{j-1}) + k_{dg} z_j + k_{fd}(z_j - y_j) - F_{f,j}(y_j - z_j) &= 0 \end{aligned} \quad . \quad (1)$$

Where the masses of the different DOFs are represented respectively as m_b, for the blade mass, m_f, for the friction dynamics mass, and m_d, for the disk sector mass. Connections between DOFs are modeled by linear springs: k_d, for the stiffness of the blade, k_{dd}, for the sector to sector stiffness, and k_{dg}, for the in-sector disk stiffness. Additionally, the spring k_{fd}, that joints the fir tree and disk sector, is added because if the fir tree and disk DFOs were connected only by the friction force, the system would be invariant to shifts of the form $x \to \Delta x, y \to \Delta y$. It is supposed that k_{fd} does not play any role

on the system dynamics. Finally, the forces acting over the system are the aerodynamic force, F_{aj}, the external excitation, $F_{forcingj}$, and the friction force, F_{fj}.

A linearized formulation of the aerodynamic forces is considered

$$\{\mathrm{F_a}\} = [K_a(\omega_0)]\{x\} + [\mathrm{C_a}(\omega_0)]\frac{d}{dt}\{x\}\,, \qquad (2)$$

and the external forcing is supposed to take the form of a travelling wave

$$F_{forcing,j} = f_j e^{i\left(\frac{2\pi EO}{N}j+\omega t\right)} + c.c. \quad (3)$$

where $c.c.$ stands for the complex conjugate.

Finally, to model the friction force, the contact at the fir-tree is assumed to remain stuck along all the friction cycle and the microslip Olofsson model (Olofsson, 1995) is used, whose friction cycle is sketched in figure 2.

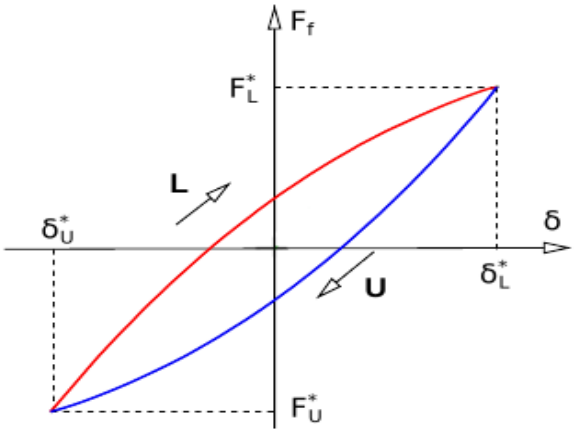

Figure 2 Olofsson microslip model: friction force for a loading-unloading cycle

The friction force is expressed, for a loading-unloading cycle, as:

$$F_f(y-z) = F_f(\delta) = F^* \pm F(\delta)\,. \quad (4)$$

where $\delta = y - z$ is the friction displacement, F^* is the friction force at the previous turning point, $+$ corresponds to the loading phase, $-$ to the unloading phase, and the increment of the friction force is given by:

$$F(\delta) = 2F_c\left(1 - \left(1 - \frac{|\delta-\delta^*|}{2\delta_c}\right)^{\frac{5}{2}}\right). \qquad (5)$$

Once the model has been presented, its parameters are adjusted to reproduce the behavior of the LPT bladed disk tested in the experiments performed in the FUTURE project. The FUTURE LPT was made of 146 sectors and presented a flat, blade dominated, first flap modal family (see the left plot of figure 3).

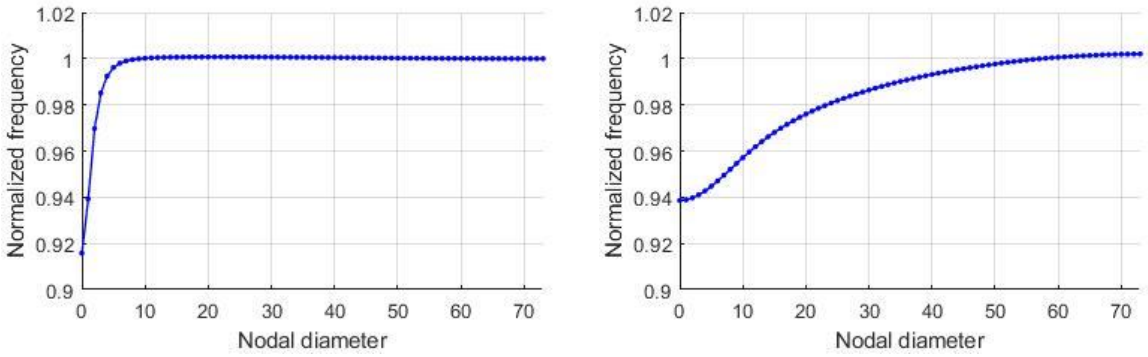

Figure 3 Tuned elastic vibration frequencies for the first flap family normalized with blade alone frequency. Left: FUTURE results (Corral et al., 2018). Right: lumped model

To replicate this modal family, the elastic parameters are set to the values presented in table 1. The frequencies obtained with the lumped model are presented in the right plot of figure 3, which are qualitatively like those from the FUTURE experiment. Because of the limitations of the lumped model the shape of the family may look different, but it shows a

similar small decay of approximately 6% between the highest (ND_{73}) and the lowest nodal diameter (ND_0) and both families are very flap.

Parameter	m_b	m_f	m_d
Value	1	0.01	1
Parameter	k_b	k_{dd}	k_{dg}
Value	1	30	10
Parameter	k_{fd}	F_c	δ_c
Value	1	1	0.1

Table 1. Values of the parameters of the lumped model

The linear aerodynamic coefficients are taken directly from the FUTURE LPT rotor. They are presented in figure 4, where it can be seen that the system has a total of 59 unstable modes and the mode corresponding to ND_{25} is the most unstable one (highlighted with a red point in figure 4).

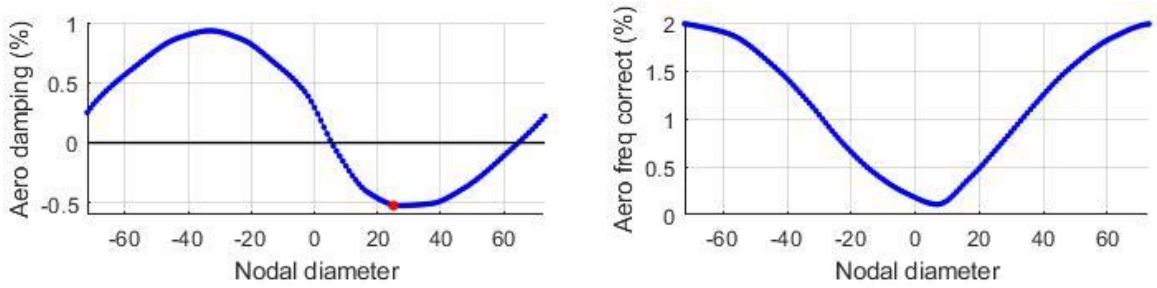

Figure 4 Aerodynamic damping (left) and frequency correction (right), from (Corral et al., 2018)

To set the friction parameters, results from flutter experiments are considered (see the red dots in figure 5). These experiments were performed with variable gas flow, in a range where it can be assumed to be proportional to the aerodynamic damping. The blade vibration amplitude obtained with the lumped model is presented in figure 5 (blue line). To obtain these results, the friction parameters presented in table 1 are used ($F_c = 1, \delta_c = 0.1$). Additionally, the material damping of the blade is added to the model by a linear damper parallel to k_b, and takes the value $\xi_{mat}/\xi_{\text{aero}} = 0.55$. As seen in figure 5, for low air flow density values this material damping suppresses the aerodynamic instability, and no flutter induced vibration is present.

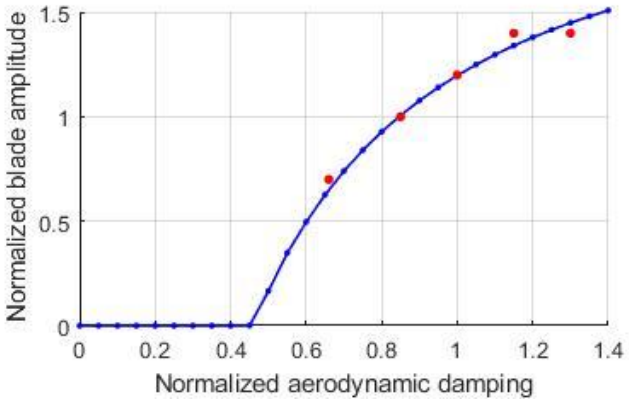

Figure 5 Mean vibration amplitude of the lumped model as a function of flow density (blue curve) and FUTURE flutter results (red dots) (Corral et al., 2018)

Finally, the level of the external forcing excitation is adjusted to the results obtained in the in-vacuum forced response tests performed in the FUTURE project, using the amplitude of the response at the resonance as the reference to calibrate the model with the experiment.

COMBINED FORCED RESPONSE AND FLUTTER RESULTS

In this section, the interaction of an aerodynamically unstable mode and a directly excited mode is studied. As mentioned, this interaction is dominated by the nonlinearity introduced by the friction at the fir-tree attachment.

Figure 6 shows a first simulation with and amplitude of the forcing of $f_j = 0.12$ and EO_{24} (which corresponds to a flutter unstable TW). Three curves are present on it; the red curve corresponds to the response of the system to the excitation force without aerodynamics (pure forced response problem), the black curve is the flutter vibration (independent of the forcing frequency), and the blue curve shows the flutter and forced response combination. In this latter case, the system does not present superposition of effects, but a clear alternation of the forced response vibration when the excitation frequency is close to the resonance, and the flutter response when the excitation frequency moves away from the resonance. This is caused by the nonlinear friction and has a beneficial effect on the vibration amplitude, producing a lower vibration level than the linear superposition of both separated effects (Corral and Gallardo, 2013).

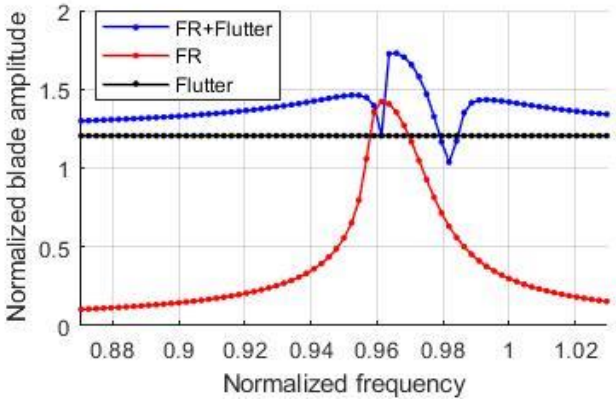

Figure 6 Blade amplitude vibration obtained with the lumped model for and excitation fj=0.12 and ND24 and nominal aerodynamic force.

Flutter response of a bladed disk with multiple aerodynamically unstable TWs presents multiple stable solutions (see (Martel et al., 2014). Each of them is composed mainly of one unstable TW (not all aerodynamically unstable TWs can conform a stable solution but only the most unstable ones), and the initial conditions determine which of these solutions will appear in the final state. Here, however, when the nodal diameter excited corresponds to an aerodynamically unstable solution, the forcing directly selects the TW which will be present in the system response. This is observed in figure 7, where the TW components of the response for two different points of the simulation in figure 6 are represented. The first point is located before the resonance, in the region where flutter dominates ($\omega_f = 0.9$), and the second in the resonance region, where the force response is dominant ($\omega_f = 0.97$). Since both effects produce a vibration of the system with the same TW, the response is dominated by this TW (TW_{24}) for all the frequency sweep.

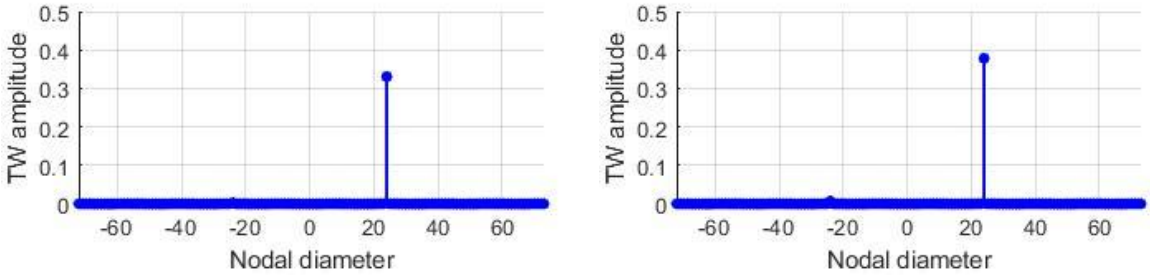

Figure 7 TWs of blade vibration for flutter and forced response case of figure 6. Left: $\omega_f = 0.9$. Right: $\omega_f = 0.97$

A second simulation is shown in figure 8, now with an excitation of $f_j = 0.09$ and EO_4. In this case, the TW directly excited is almost aerodynamically neutral and, thus, it does not correspond to a stable solution to flutter. Because of this, in the region away from the resonance that is dominated by the flutter, another TW which is not directly excited by the external forcing shows up in the response (TW_{24}, see figure 9) and, unlike in the previous case, the response is no longer composed by a single TW. On the flutter dominated region, both the flutter TW and the directly excited TW are present, as well as their combinations with a much smaller amplitude (see figure 9 on the left). On the other hand, near the resonance, flutter is suppressed and the response is again mainly composed by the TW directly excited by the forcing (TW_4) and its small nonlinear echoes (see figure 9 on right).

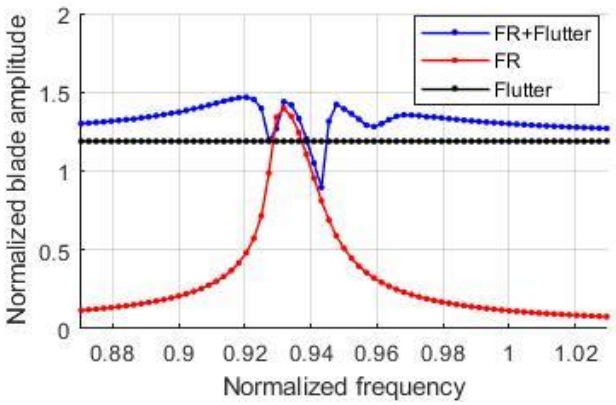

Figure 8 Blade amplitude vibration obtained with the lumped model for and excitation fj=0.09 and ND4 and nominal aerodynamic force.

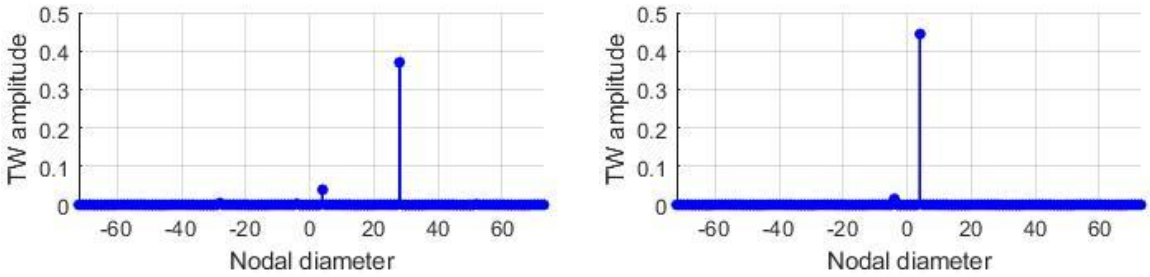

Figure 9 TWs of blade vibration for flutter and forced response case of figure 8. Left: $\omega_f = 0.87$. Right: $\omega_f = 0.93$

It is interesting to mention that the kinks in the forced response plus flutter curve of figure 8 are not present in the forced response plus flutter curve of figure 6. The reason for this difference is the fact that the TW directly excited by the forcing in the first case is the same TW that grows because of flutter, and thus, there is only one TW involved in the response of the system throughout all the frequency sweep. The second case has a more complex dynamics as the TW directly excited and the TW generated by the flutter instability are different TWs. Because of this, there is a region after the resonance peak where both TWs interact, producing the kinks shown in the amplitude.

TWO COMBINED EXTERNAL FORCINGS

In this section, the case where two external forcings excite simultaneously the system is studied. The forces considered have different nodal diameters and different frequencies, but both excite the same modal family (in this case the first one).

It is important to point out that the vibration amplitude reached when two forced responses are present in the problem is higher than that obtained in the interaction between flutter and forced response. As mentioned, the friction of the model was calibrated with data from FUTURE flutter tests (Corral et al., 2018), and, if the same forcing amplitudes than in the previous section were used, the resulting displacements would grow into the macroslip regime close to the resonance peaks. To remain into the microslip regime throughout all the simulations, the excitation levels of both forcings have been reduced.

On figure 10, the results obtained applying one forcing with high engine order (trying to mimic flutter), $f_{1j} = 0.03$ and EO_{24}, and another with low engine order, $f_{2j} = 0.03$ and EO_4, are shown. The blue curve corresponds to a case where the low engine order excitation is almost not present, and it essentially corresponds to the forced response of the system to only the first excitation with EO_{24}. On top of this curve, plotted with a red line and starting from the resonance of the previous curve, it is represented the frequency sweep of the second forcing with EO_4. The response is basically a superposition of both separated forced responses, and no alternation of effects is observed on the solution in this case. The only effect of the modal interaction that can be appreciated is a reduction of the amplitude at the simultaneous resonance of both forcings with respect to the linear superposition (this effect is mainly due to the nonlinear friction saturation of the displacement for the applied forcing)

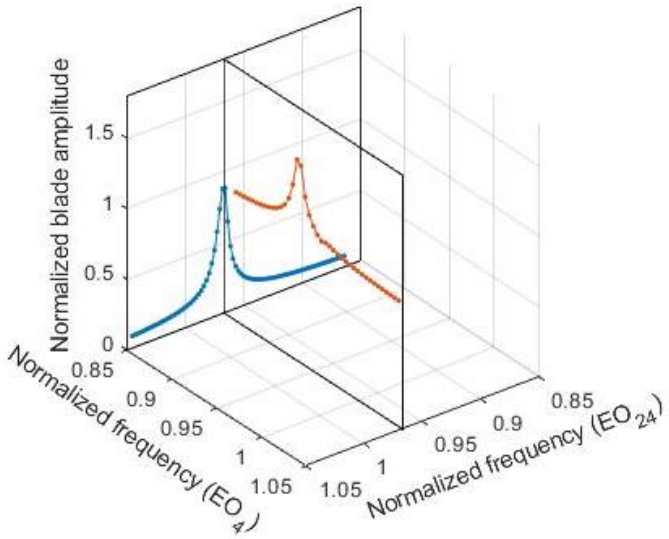

Figure 10 Blade vibration amplitude obtained with the lumped model for two forced response cases with EO24 and EO4 and fj=0.03

Figure 11 shows the TW components of the response at the simultaneous resonance of both forcings. As expected, the response is mainly composed of the two TW directly excited by the two forcings, and only a small contribution is produced by their nonlinear combination.

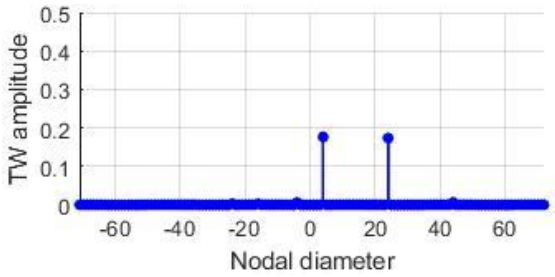

Figure 11 TWs of the blade vibration for the two forced response case of figure 10 at the resonance of both forcings.

As a final comment, all the simulations performed, although integrated in time using a second order explicit scheme, have a low computational cost due to the reduced order of the lumped model used. A total of 500 elastic cycles have been integrated for each frequency requiring around 10^4 $seconds$ in a computer with 4 Intel® Core™ i7-7700 processors.

CONCLUSIONS

A mass-spring model with 3 DOF per sector has been introduced and adjusted using the results from the LPT flutter and forced response experiments performed in the FUTURE project. This reduced order model has been used to analyze the nonlinear modal interaction caused, firstly, by the simultaneous presence of flutter and forced response, and, secondly, by two forced responses. The results obtained allow us to draw the following final remarks:

- For the simultaneous case of forced response and flutter, the response of the system does not correspond to the direct superposition of the two separated effects. There is a clear alternation of effects: close to the resonance peak, the forced response vibration is dominant, while away from resonance the flutter instability sets in.
- If the forcing excites a TW that has a high aerodynamic instability, this TW will be triggered by the forcing away from the resonance region and, basically, the response of the system will be composed of the same TW for all the frequency sweep.
- If, on the other hand, the forced TW does not have a high flutter instability, then a different, more unstable TW will arise on the flutter dominated region of the frequency sweep away from the resonance.
- There is no alternation of effects in the case with two forcings. The only nonlinear effect close to the simultaneous resonance of both excitations is the saturation of the vibration amplitude due to the friction, that produces a final vibration amplitude that is reduced with respect to the linear superposition case.
- The combined effect of two forcings does not appear to have similar dynamics as the combination of flutter and forced response. This can be understood considering the fundamental differences between these two types of

phenomena. While flutter is an instability phenomenon that depends on the response of the system itself, the forced response vibration is caused by an external forcing. Indeed, in the case of flutter, the null solution always exists (although it could be unstable), this is not true in the forced response case, where the system always shows a response to the external excitation.

NOMENCLATURE

DOF	Degree of Freedom
EO	Engine order
HCF	High Cycle Fatigue
ND	Number of nodal diameters
ROM	Reduced Order Model
TW	Travelling Wave
c.c.	Complex conjugate

ACKNOWLEDGMENTS

This work has been supported by the Advanced Research Into Aeromechanical Solutions (ARIAS) project of the European Union's Horizon 2020 research and innovation program (grant agreement No 769346). The work of CM has also been supported by the Spanish Ministerio de Economía, Industria y Competitividad under grant DPI2017-84700-R.

BIBLIOGRAPHY

Corral, R., Beloki, J., Calza, P., and Elliott, R. Flutter generation and control using mistuning in a turbine rotating rig. *AIAA Journal*, 57:1–14, 10 2018.

Corral, R. Gallardo, J.M., Conceptual Analysis of the Non-Linear Forced Response of Aerodynamically Unstable Bladed-Discs, Proceedings of the ASME Turbo Expo. 2013: 7.10.1115/GT2013-94851

Cowles, B.A. High cycle fatigue in aircraft gas turbines—an industry perspective. *Int J Fract* 80, 147–163 (1996). https://doi.org/10.1007/BF00012667

Gross, J. and Krack, M. Multi-wave vibration caused by flutter instability and nonlinear tip shroud friction. *Journal of Engineering for Gas Turbines and Power*, 09 2019.

Krack, M., Salles, L., and Thouverez, F., "Vibration Prediction of Bladed Disks Coupled by Friction Joints," Archives of Computational Methods in Engineering, Vol. 24, 2017, pp. 589–636.

Olofsson, U. Cyclic microslip under unlubricated conditions. *Tribology International*, 28:207–217, 1995

Martel, C., and Martín, J. A. (December 12, 2019). "Asymptotic Description of Forced Response Vibration Saturation by Friction Forces." ASME. J. Eng. Gas Turbines Power. January 2020; 142(1): 011022.

Martel, C., Corral, R. and Ivaturi, R. Flutter amplitude saturation by nonlinear friction forces: Reduced model verification. *Journal of Turbomachinery*, 137(4):041004–041004–8, Oct 2014.

Petrov, E. P., and Ewins, D. J., "Analytical Formulation of Friction Interface Elements for Analysis of Nonlinear Multi-Harmonic Vibrations of Bladed Disks," Journal of Turbomachinery, Vol. 125, No. 2, 2003, pp. 364–371.

Petrov, E. P., and Ewins, D. J., "State-of-the-art dynamic analysis for non-linear gas turbine structures," Proceedings of the Institution of Mechanical Engineers, Part G: Journal of Aerospace Engineering, Vol. 218, No. 3, 2004, pp. 199–211.

Sinha, A. Vibration of nearly periodic structures and mistuned bladed rotors. Cambridge University Press (2017) 10.1017/9781316986806.B.A.

Yang, B.D., Chu, M.L. and Menq, C.H. Stick-slip separation analysis and non-linear stiffness and damping characterization of friction contacts having variable normal load. *Journal of Sound and Vibration*, 210(4): 461–481,1998.

Yang, B.D. and Menq, C.H. Characterization of 3d contact kinematics and prediction of resonant response of structures having 3d frictional constraint. *Journal of Sound and Vibration*, 217(5): 909–925, 1998.